Mechanical properties of copper nanocube under three-axial tensile loadings

Yang Zai-Lin(杨在林)†, Zhang Guo-Wei(张国伟), and Luo Gang(罗 刚)

College of Aerospace and Civil Engineering, Harbin Engineering University, Harbin 150001, *China*

(Received 12 November 2014; revised manuscript received 7 January 2015; published online 10 April 2015)

The mechanical properties of copper nanocubes by molecular dynamics are investigated in this paper. The [100], [110], [111] nanocubes are created, and their energies, yield stresses, hydrostatic stresses, Mises stresses, and the relationships between them and strain are analyzed. Some concepts of the microscopic damage mechanics are introduced, which are the basis of studying the damage mechanical properties by molecular dynamics. The [100] nanocube exhibits homogeneity and isotropy and achieves a balance easily. The [110] nanocube presents transverse isotropy. The [111] nanocube shows the complexity and anisotropy because the orientation sizes in three directions are different. The broken point occurs on a surface, but the other two do not. The [100] orientation model will be an ideal model for studying the microscopic damage theory.

Keywords: molecular dynamics, damage, three-axial tensile loading, isotropy

PACS: 62.25.–g, 61.46.–w, 81.07.Nb **DOI:** 10.1088/1674-1056/24/6/066203

1. Introduction

In the past decade, nanocrystalline materials[1] have been the focus of intense research because of their unusual mechanical properties, and a lot of methods[2] have been used to investigate the nanocrystalline materials, such as experiments, the Monte Carlo method, the molecular dynamics method, and coupling with each other.[3] Due to the development of computer technology, molecular dynamics simulation (MD) is widely used to study the characteristics of nanocrystalline materials, including nanowire, nanoscale void, nanoscale surface damage, radiation damage, nanofilms, etc.

Temperature, orientation, tensile rate, anisotropic, size effects affect the breaking behavior of nanoscale structures under uniaxial tensile loading.[4–9] Then the void growth and coalescence in single crystal nickel show the length effect on the void.[10] In addition, with void growing research receiving attention, defects with twin boundaries,[11] defects in collision cascades,[12] etc. were published. In recent years, surface modification, damage formation,[13,14] and nanofilms[15] are attractive popularly. Furthermore, in the nuclear field, radiation damages are studied extensively. With the demand of engineering, the gap between the macromechanics and micromechanics is gradually becoming smaller. Continuum-like deformation and stress is a new method[16] of simulating the molecular dynamics. The mechanics across the scales attracts many researchers, and the combined molecular dynamics–micromechanics method[17] is employed to consider the stiffness of nanocomposites. This paper is to establish the relationship between mesomechanics and micromechanics.

Nevertheless, when nanoscale structures are studied, they are always compared with macroscopic mechanical properties. In this case, uniaxial tensile loading can solve some problems inadequately. The uniaxial stress state cannot solve the comprehensive stress, which leads to the structure breaking. Three-dimensional (3D) molecular dynamics simulations are taken into account. Reference [18] discussed the 3D MD simulations, whose analysis is still in the plane. The mechanical properties of copper nanocube are investigated under three-axial tensile loading for overcoming the shortage, and the mechanical properties are fully analyzed.

The rest of this paper is organized as follows. In Section 2, we create the model and method. The results will be discussed in Section 3. Finally, some conclusions are drawn from the present study in Section 4.

2. Model and method

2.1. Molecular dynamics simulations and models

Molecular dynamics simulations are performed with the software NanoMD,[19] which is developed by Zhao's group (Nanjing University), through improving the models for simulation. The models are [100], [110], [111] nanocubes, whose sizes are all $20a$ (a denotes the copper lattice constant that is 0.3615 nm) corresponding to 34461, 33341, and 32239 atoms respectively under three-axial tensile loadings (Fig. 1).

There are tensile atoms whose sizes are a in models, and the tensile atoms without mutual coupling in three directions ensure the independence of tensile loadings in three directions (Fig. 1(a)). Also, there are tensile atoms only in the z direction when the model is loaded under uniaxial tension. Figure 1(b) shows the schematics of three orientations' models in x, y, and z directions.

†Corresponding author. E-mail: yangzailin00@163.com

© 2015 Chinese Physical Society and IOP Publishing Ltd

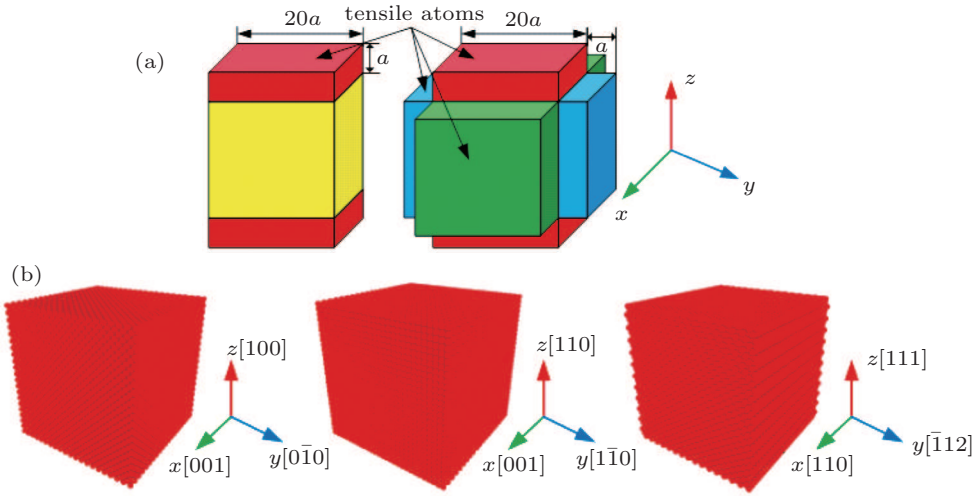


Fig. 1. (color online) (a) Sketches of nanocubes under uniaxial and three-axial tensile loadings, (b) schematic diagram of crystallographic orientations of three nanocubes under three-axial tensile loadings.

In this work, MD simulations are carried out with the embedded-atom method (EAM) potential developed by Johnson,[20] which could provide an effective description of the transition metals with a face-centered cubic (FCC) structure. The total energy[21] is given by

$$E_{\rm tot} = \sum_i E_i, \tag{1}$$

$$E_i = F_i(\rho_i) + \frac{1}{2}\sum_{j\neq i}\phi_{ij}(r_{ij}), \tag{2}$$

$$\rho_i = \sum_{j\neq i} f_j(r_{ij}), \tag{3}$$

where $E_{\rm tot}$ is the total internal energy of an assembly of atoms, E_i is the internal energy of atom i, ρ_i is the electron density contribution of all other atoms at atom i, $F_i(\rho_i)$ is the energy to embed atom i into the electron density ρ_i, r_{ij} is the distance between atoms i and j, $\phi_{ij}(r_{ij})$ is the pair potential with the distance between atoms i and j being r_{ij}, and $f_j(r_{ij})$ is the contribution of the atom j at r_{ij} to the electron density at atom i. The potential with the nearest neighbor atom model is used. The pair potential and the embedded energy are given[22] by

$$\phi(r) = \phi_{\rm e}\exp\left[-\gamma\left(\frac{r}{r_{\rm e}}-1\right)\right], \tag{4}$$

$$F(\rho) = -E_{\rm c}\left[1-\frac{\alpha}{\beta}\ln\left(\frac{\rho}{\rho_{\rm e}}\right)\right]\left[\frac{\rho}{\rho_{\rm e}}\right]^{\alpha/\beta} - 6\phi_{\rm e}\left[\frac{\rho}{\rho_{\rm e}}\right]^{\gamma/\beta}, \tag{5}$$

where $E_{\rm c}$, $\phi_{\rm e}$, α, β, and γ are the parameters of EAM potentials for FCC metal. The variables with subscript e refer to the equilibrium values of the variables.

During the simulations the number of atoms, the volume and the energy of systems are invariant, corresponding to micro-canonical ensemble in statistical mechanics. The models set 2×10^4 relaxation steps at 30 K at the beginning. The atomic velocity of the models in accordance with Gaussian random number can correspond to the Maxwell–Boltzmann velocity[23] through relaxation. Then by atomic velocity correction the systems work up to thermal equilibrium states. For stress veracity, when the stresses are all less than 0.01 GPa, the relaxation process stops. After enough relaxation, the tensile atoms of the models are stretched by 0.01% ps^{-1} under three-axial tension. The simulation uses a combined Verlet leapfrog and cell-linked list algorithm. Above all, the simulation can reveal some mechanical quantities.

2.2. Mechanical quantities

The stress is computed by the virial scheme, and the overall stress is averaged over all atomistic stresses. For the system, the corresponding stress in the n direction is the average stress of the plane atoms, which is perpendicular to the n direction. The corresponding atomic stress is expressed in terms of EAM potential functions as follows:[24]

$$\sigma_i^{\xi\eta} = \frac{1}{\Omega_i}\left\{-m_i v_i^{\xi} v_i^{\eta} + \frac{1}{2}\sum_{j\neq i}\left[\frac{\partial\phi}{\partial r_{ij}} + \left(\frac{\partial F}{\partial\rho_i}+\frac{\partial F}{\partial\rho_j}\right)\frac{\partial f}{\partial r_{ij}}\right]\frac{r_{ij}^{\xi} r_{ij}^{\eta}}{r_{ij}}\right\}, \tag{6}$$

where $\sigma_i^{\xi\eta}$ is the $\xi\eta$ component of the atomic stress tensor of atom i, Ω_i is the average volume of atom i, m_i is the mass of atom i, v_i^{ξ} and v_i^{η} are the velocity components in the ξ and η direction of atom i respectively, r_{ij}^{ξ} and r_{ij}^{η} are the displacement components in the ξ and η directions of r_{ij} respectively.

The strain ε is defined as $\varepsilon = (l-l_0)/l_0$, where l is the length of the current model, and l_0 is the length of the model after relaxation. Like the case in macro-mechanics, hydrostatic stress $\sigma_{\rm m}$ and Mises stress $\sigma_{\rm eq}$ are defined respectively as follows:

$$\sigma_{\rm m} = \frac{1}{3}(\sigma_1+\sigma_2+\sigma_3) = \frac{1}{3}(\sigma_x+\sigma_y+\sigma_z), \tag{7}$$

$$\sigma_{\rm eq} = \sqrt{\frac{1}{2}\left[(\sigma_1-\sigma_2)^2+(\sigma_2-\sigma_3)^2+(\sigma_3-\sigma_1)^2\right]}$$

$$= \sqrt{\frac{1}{2}\left[(\sigma_x-\sigma_y)^2+(\sigma_y-\sigma_z)^2+(\sigma_z-\sigma_x)^2\right]}, \quad (8)$$

where σ_1, σ_2, and σ_3 are principal stresses, σ_x, σ_y, and σ_z are the stresses in the three directions. Shear stress does not exist, so σ_1, σ_2, and σ_3 can be replaced by σ_x, σ_y, and σ_z.

The Gurson damage model has given four models containing voids, and the model of spherical voids will meet the yield surface equation:[25]

$$\left(\frac{\sigma_{\rm eq}}{\sigma_{\rm s}}\right)^2 + 2h\cosh\left(\frac{3\sigma_{\rm m}}{2\sigma_{\rm s}}\right) - 1 - h^2 = 0, \quad (9)$$

where $\sigma_{\rm s}$ is the yield stress, and h is the volume percentage of the void. When h is a constant value, the equation is the relationship between $\sigma_{\rm eq}$ and $\sigma_{\rm m}$ because $\sigma_{\rm s}$ always is a constant value.

3. Result and discussion

3.1. Energies in different crystal orientation models

Figure 2 gives the average kinetic energies and potential energies under uniaxial and three-axial tensile loadings. According to thermodynamic kinetic energy formula $E_{\rm ke} = 3/2k_{\rm B}NT$, where $k_{\rm B}$, N, and T are the Boltzmann constant, the total number of atoms, and the thermodynamic temperature respectively. The average kinetic energy can be affected only by T. As seen in Fig. 2, the average kinetic energies decrease suddenly and the average potential energies increase with tension increasing after enough relaxation. The average potential energies become different under uniaxial and three-axial tension. Under the three-axial tension, the average potential energies have no obvious secondary peaks (A, B, and C points) (see Figs. 2(a) and 2(b)). The relaxation steps are 20773, 25629, and 26181 steps for [100], [110], and [111] nanocubes. Although this figure is unlikely to be entirely accurate, it can show that the [111] nanocube has bigger stress and enters into the small stress state, and turns harder than the nanocubes of the other two orientations. In other words, the configuration of the [111] nanocube is more difficult to break and more stable than the nanocubes of the other two orientations.

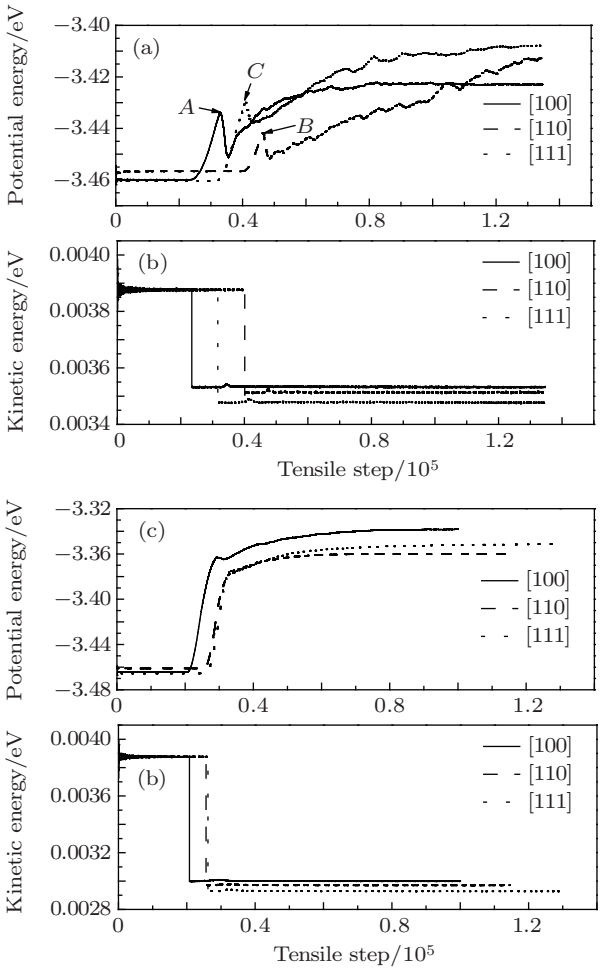


Fig. 2. Average kinetic energies and potential energies of different orientations under (a) and (b) uniaxial and (c) and (d) three-axial tensile loadings.

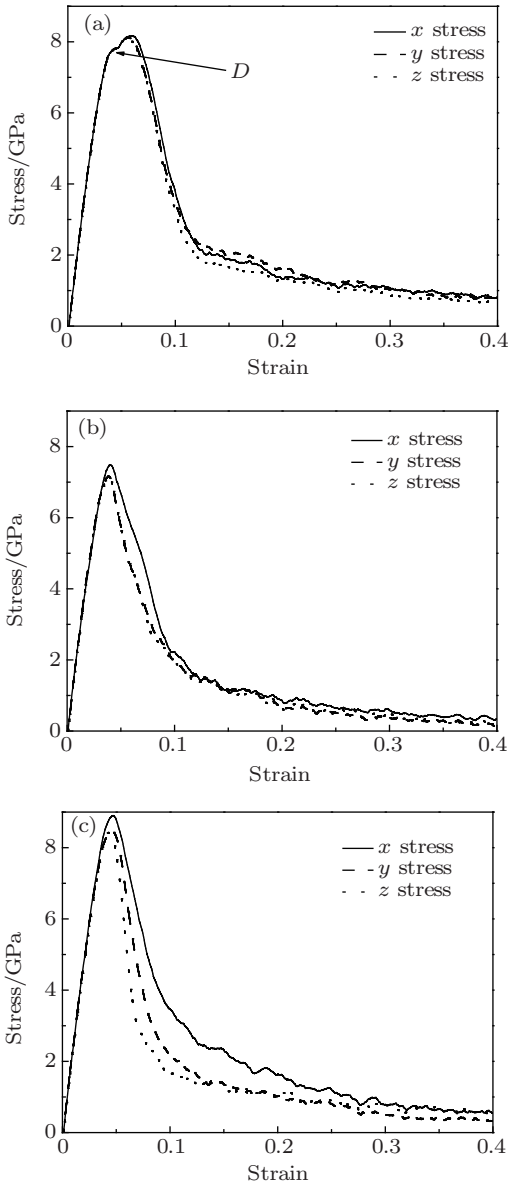


Fig. 3. Stress-strain curves of (a) [100] oriented nanocube, (b) [110] oriented nanocube, and (c) [111] oriented nanocube.

3.2. Stresses in models of different crystal orientations

When the [100], [110], and [111] models are under three-axial tension, the different mechanical properties are displayed in three tensile directions. Figure 3 exhibits the stress–strain curves of the models of the three orientations.

All curves exhibit mechanic properties like the macromechanic ones. However, only the [100] nanocube shows the obvious yield stage (D point) and its three curves are almost coincident (see Fig. 3(a)). The x axial curve is different from the other two curves in the [110] nanocube. In the [111] nanocube, three curves are not coincident except in elastic stages. Some detailed mechanical parameters are shown in Table 1.

Table 1. Some detailed numerical values of three crystal orientations in three tensile directions.

	[100]			[110]			[111]		
	x [001]	y [010]	z [100]	x [001]	y [$1\bar{1}0$]	z [110]	x [$1\bar{1}0$]	y [$11\bar{2}$]	z [111]
Yield stress/GPa	8.17025	8.12366	8.11275	7.48015	7.16021	7.12707	8.90265	8.44737	8.42338
Yield strain	0.05943	0.05693	0.05493	0.03947	0.03867	0.03886	0.04705	0.04620	0.04280
Tensile step	5943	5693	5493	3947	3867	3886	4705	4620	4280
Orientation size[a]	$a/2$	$a/2$	$a/2$	$a/2$	$\sqrt{2}a/4$	$\sqrt{2}a/4$	$\sqrt{2}a/4$	$\sqrt{6}a/4$	$\sqrt{3}a/3$

[a]Orientation size in the n direction is defined as the projection direction of atoms in the n direction.

From Table 1, the orientation size affects the yield stress because the stress is given from the statistical average theory. The orientation sizes are similar in the [100] nanocube, so the yield stresses are similar. In the [110] nanocube, yield stress is in proportion to orientation size in the case of ignoring the small error. However, the [111] nanocube is too difficult to forecast the relationship between orientation size and stress because the orientation size is not unique in different planes. Figure 3 shows that in the elastic stage the three stress-strain curves are overlapping in each orientation model. So the Young moduli are similar in the crystal orientation models.

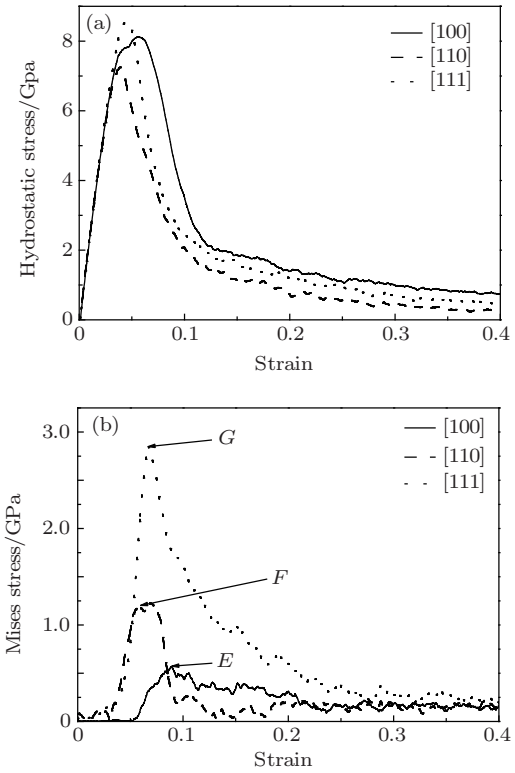


Fig. 4. Stress–strain curves of nanocubes of different crystal orientations: (a) hydrostatic stress and (b) Mises stress.

Hydrostatic stress is the stress averaged over the stresses in three directions. Young's modulus calculated by the hydrostatic stress–strain curve is about 185 GPa in Fig. 4(a). Mises stress comprehensively considers the influence of the principal stress on the yield strength. Figure 4(b) displays the relationship between Mises stress and strain. With the tensile loadings the Mises stresses first smoothly change then increase quickly, and finally decrease. Like the case in macromechanics, the material also has an elastic stage, yield stage, and fracture stage. The peaks (E, F, G) explain the effect of the orientation size on the stresses in three directions. The hydrostatic stress and Mises stress display the integrity and difference in stress among the three directions.

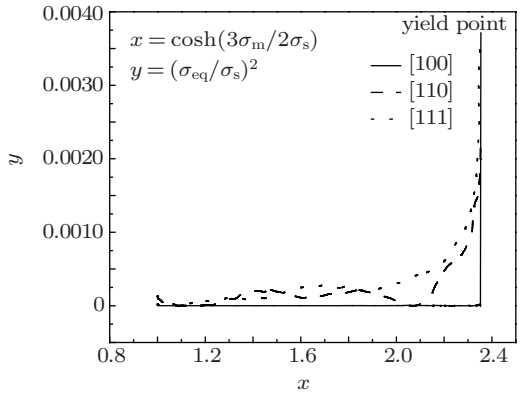


Fig. 5. Mises stress–hydrostatic stress curves of three crystal orientations.

For the Gurson damage model, we need to consider the relationship between the Mises stress and the hydrostatic stress (Fig. 5). When the model has no void, the diagram of y–x should be a straight line. In this case, Mises stress is unrelated to the hydrostatic stress. However, from Fig. 5, it can be understood that only the [100] crystal orientation curve is almost a straight line. The curves are related to not only the void per-

centage but also orientation sizes. When the hydrostatic stress nearly reaches the yield points, the Mises stress increases more rapidly in the [111] nanocube than the [110] nanocube, and hardly increases in the [100] nanocube. Isotropy is essential to study the microscopic damage.

3.3. Break properties

As is well known, when the stress is over yield stress, the models start to break and the stress decreases rapidly. From the above analysis, the yield points of the models of three orientations are different.

Three crystal orientations' relaxation steps and yield steps are 20773 and 26351 in the [100] nanocube, 25629 and 29557 in the [110] nanocube, 26181 and 30786 in the [111] nanocube. Figure 6 shows the stress increasing processes of different nanocubes, where the number and distribution of atoms explain the stress trend of different nanocubes.

For the [100] nanocube, the orientation sizes are the same, homogeneities are clearly present in tensile processes. The atoms around the [100] nanocube corners firstly begin to change and extend to the edges little by little. For the [110] nanocube, their edges change their origins, which is different from the case for the [100] nanocube. Dislocations appear in the edges on the [100] and [110] nanocubes. However, z-plane atoms start to slip in the [111] nanocube at the beginning of loadings, which is completely different from those in the former two kinds of nanocubes.

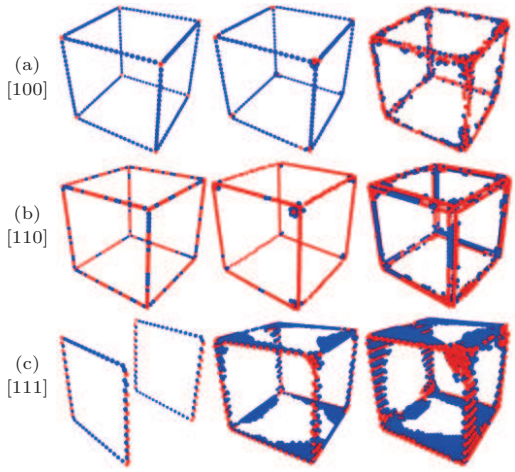


Fig. 6. (color online) Stress increasing processes of (a) [100], (b) [110], (c) [111] nanocubes.

Figure 7 shows that different dislocations cause the different broken states of three crystal orientations. The 45° dislocation of the [100] nanocube verifies its isotropy fully, and broken states in three directions are almost the same. In the [110] nanocube, the gaps first appear on the edges, then three dislocations display with tensile loadings. Finally, gliding along 45° leads to the breaking of the [110] nanocube. The [111] nanocube's glide and broken plane is about 60° angle with respect to the x axis. Combining with the previous discussion, it can be seen that the z plane is almost broken and the x plane is hardly broken. The y-axis atoms are out of the model earliest. Therefore, different orientation sizes lead to different dislocations and form different broken states.

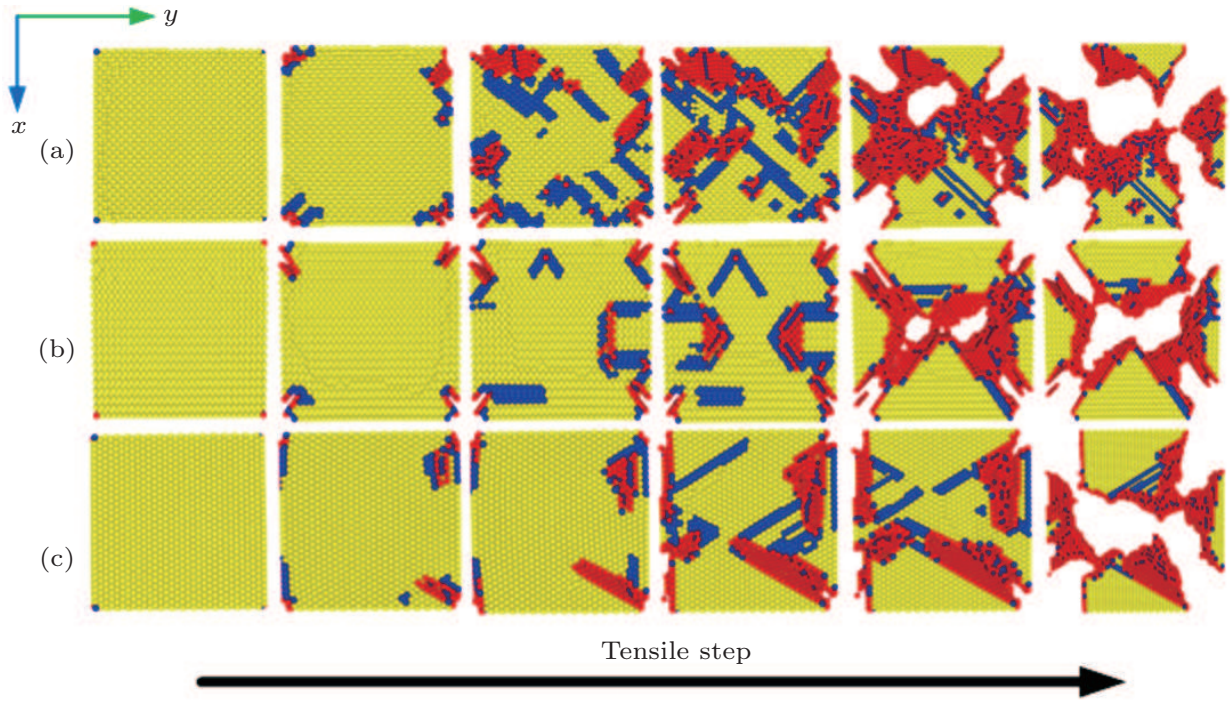


Fig. 7. (color online) Dislocation states of (a) [100], (b) [110], and (c) [111] nanocubes with tensile step.

4. Conclusions

In this paper, mechanical properties of the [100], [110], and [111] nanocubes are investigated by molecular dynamics simulation under three-axial tensile loadings. The results of the simulation explain that [100], [110], and [111] nanocubes present isotropy, transverse isotropy, and anisotropy respectively due to the different orientation sizes. The nanocube yield process is short under three-axial tension. It is the basic mechanical properties that hydrostatic stress can reflect the whole stress level of nanocubes. Mises stress must be taken into account when directionality is considered, which can fully reflect the influences of the principal stress on each other. The results can be the research foundation ranging from mesoscopic damage mechanics to microscopic damage mechanics.

References

[1] Meyers M A, Mishra A and Benson D J 2006 *Prog. Mater. Sci.* **51** 427

[2] Frenkel D and Smit B 2001 *Understanding Molecular Simulation: from Algorithms to Applications*, Vol. 1 (Beijing: Science Press) pp. 18–86 (in Chinese)

[3] Gao Y, Wang H, Zhao J, Sun C and Wang F 2011 *Comput. Mater. Sci.* **50** 3032

[4] Zhao J, Murakoshi K, Yin X, Kiguchi M, Guo Y, Wang N, Liang S and Liu H 2008 *J. Phys. Chem. C* **112** 20088

[5] Liu Y, Zhao J and Wang F 2009 *Phys. Rev. B* **80** 115417

[6] Huang D and Zhuo J S 2006 *Computational Methods in Engineering and Science EPMESC X*, August 21–23, 2006, Sanya, Hainan, China, p. 839

[7] Yokomizo K, Banno Y and Kotaki M 2012 *Polymer* **53** 4280

[8] Liu Y and Zhao J 2011 *Comput. Mater. Sci.* **50** 1418

[9] Zhao J, Hou J, Zhu T, Wang F, Liu Y and Yin X 2010 *Comput. Mater. Sci.* **47** 962

[10] Potirniche G P, Horstemeyer M F, Wagner G J and Gullett P M 2006 *Int. J. Plast.* **22** 257

[11] Hussain F, Hayat S S, Shah Z A, Hassan N and Ahmad S A 2013 *Chin. Phys. B* **22** 096102

[12] Devanathan R, Corrales L R, Weber W J, Chartier A and Meis C 2005 *Nucl. Instrum. Method Phys. Res. B* **228** 299

[13] Aoki T and Matsuo J 2006 *Nucl. Instrum. Method Phys. Res. B* **242** 517

[14] Chen R, Liang M, Luo J, Lei H, Guo D and Hu X 2011 *Appl. Surf. Sci.* **258** 1756

[15] Heino P 2007 *Eur. Phys. J. B* **60** 171

[16] Zhang L, Jasa J, Gazonas G, Jérusalem A and Negahban M 2014 *Comput. Methods Appl. Mech. Eng.* **283** 1010

[17] Shokrieh M M, Shokrieh Z and Hashemianzadeh S M 2014 *Mater. Des.* **64** 96

[18] Li J, Fang Q, Liu Y and Zhang L 2014 *Appl. Surf. Sci.* **303** 331

[19] Zhao J, Yin X, Liang S, Liu Y, Wang D, Deng S and Hou J 2008 *Chem. Res. Chin. Univ.* **24** 367

[20] Johnson R A 1988 *Phys. Rev. B* **37** 6121

[21] Johnson R A 1988 *Phys. Rev. B* **37** 3924

[22] Johnson R A 1989 *Phys. Rev. B* **39** 12554

[23] Long Z, Xu W and Tang L 2007 *Molecular Simulation Theory and Practice*, Vol. 1 (Beijing: Chemical Industry Press) pp. 79–81 (in Chinese)

[24] Wu H 2006 *Eur. J. Mech. A-Solid* **25** 370

[25] Gurson A L 1977 *J. Eng. Mater. Tech.* **99** 2